

$I = 2$ $\pi\pi$ scattering phase shift from the HAL QCD method with the LapH smearing

Daisuke Kawai,¹ Sinya Aoki,² Takumi Doi,^{3,4} Yoichi Ikeda,⁵ Takashi Inoue,⁶
Takumi Iritani,³ Noriyoshi Ishii,⁵ Takaya Miyamoto,² Hidekatsu Nemura,⁵ and Kenji Sasaki²

(HAL QCD Collaboration)

¹*Department of Physics, Kyoto University, Kyoto 606-8502, Japan*

²*Center for Gravitational Physics, Yukawa Institute for Theoretical Physics,
Kyoto University, Kyoto 606-8502, Japan*

³*Theoretical Research Division, Nishina Center, RIKEN, Saitama 351-0198, Japan*

⁴*iTHEMS Program and iTHES Research Group, RIKEN, Wako 351-0198, Japan*

⁵*Research Center for Nuclear Physics (RCNP),
Osaka University, Osaka 567-0047, Japan*

⁶*Nihon University, College of Bioresource Sciences, Kanagawa 252-0880, Japan*

(Dated: March 8, 2022)

Abstract

Physical observables, such as the scattering phase shifts and the binding energies, calculated from the non-local HAL QCD potential do not depend on the sink operators used to define the potential. This is called the scheme independence of the HAL QCD method. In practical applications, the derivative expansion of the non-local potential is employed, so that physical observables may receive some scheme dependence at given order of the expansion. In this paper, we compare the $I = 2$ $\pi\pi$ scattering phase shifts obtained in the point-sink scheme (the standard scheme in the HAL QCD method) and the smeared-sink scheme (the LapH smearing newly introduced in the HAL QCD method). Although potentials in different schemes have different forms as expected, we find that, for reasonably small smearing size, the resultant scattering phase shifts agree with each other if the next-to-leading order (NLO) term is taken into account. We also find that the HAL QCD potential in the point-sink scheme has negligible NLO term for wide range of energies, which implies a good convergence of the derivative expansion in this case, while the potential in the smeared-sink scheme has non-negligible NLO contribution. Implication of this observation to the future studies of resonance channels (such as the $I = 0$ and 1 $\pi\pi$ scatterings) with smeared all-to-all propagators is briefly discussed. All computations in this paper have been performed at the lattice spacing $a \simeq 0.12$ fm ($1/a \simeq 1.6$ GeV) on a $16^3 \times 32$ lattice with the pion mass $m_\pi \simeq 870$ MeV.

I. INTRODUCTION

Understanding the spectra of hadrons including resonant states from the fundamental theory, quantum chromodynamics (QCD), is one of the major goals in particle and nuclear physics. Lattice QCD is a well-established approach as the first-principles calculation of QCD: The calculation of the spectra of the ground state of the single hadron has been matured and it is an important next challenge to determine interactions between hadrons, which are essential to study the hadron-hadron scatterings and properties of resonances such as ρ and Δ . In lattice QCD, hadron-hadron interactions are mainly investigated by two methods. The first one is the Lüscher's finite volume method [1] and its extensions [2–5]. In this approach, the energies of the states on finite volume lattices are extracted from temporal correlation functions and are converted to the scattering phase shifts in the infinite volume through the Lüscher's finite volume formula [1]. This method has been applied to the meson-meson interactions not only in non-resonant channels but also in resonant channels such as ρ , a_0 and σ [6–12], by using the advanced numerical techniques including the variational method [13, 14] and all-to-all propagators. The second method is the HAL QCD method [15–17], in which non-local but energy-independent potentials are extracted from the space-time dependence of the Nambu-Bethe-Salpeter (NBS) wave functions. Physical observables such as phase shifts and binding energies are then obtained by solving the Schrödinger equation using the HAL QCD potentials. This method is also applied for wide range of hadron systems [18–30] including the candidate of exotic tetraquark resonance, $Z_c(3900)$ [31]. While HAL QCD method has been mainly used for channels in which a so-called disconnected diagram is absent, it can be also applied for systems with disconnected diagrams, which are typical for resonant channels, by incorporating a method to calculate all-to-all propagators with an affordable computational cost. In this work, we perform a lattice QCD calculation of $I = 2$ $\pi\pi$ scatterings from the HAL QCD method with the Laplacian Heaviside (LapH) method (or distillation) [35, 36] to calculate all-to-all propagators, as a first step toward the future studies of resonant states such as ρ and σ .

With the use of the LapH method, the operator is automatically smeared. It is then of importance to study the dependence of results on the smearing of operators, since the NBS wave function and the potentials are defined by the sink operators in the HAL QCD method. Theoretically, the physical observables extracted from non-local potentials are independent

of the definition of sink operators (such as smearing) even though the form of potentials itself will vary depending on the operators [19, 32–34]. We call this fact as “scheme independence of HAL QCD method”. In the practical calculations, however, derivative expansion in terms of the non-locality of the potential is employed, so that some sink operator dependence might appear in physical observables for a given order of the expansion. In this study, we investigate the scheme independence in the HAL QCD method, by comparing the phase shifts extracted from the potential defined with point sink operator (“point-sink scheme”), which is standard operator in HAL QCD method, with those defined with smeared sink operator (“smeared-sink scheme”). In order to make a precise investigation, we consider the $I = 2 \pi\pi$ scattering as a benchmark system. The $I = 2 \pi\pi$ scattering phase shifts are well-studied by experiments [37–39] and lattice calculations by using Lüscher’s finite volume method [40, 41]. Moreover, the calculation of NBS wave functions for this channel can be done in an affordable cost even with point-sink scheme because the propagation of quarks in the same time slice is absent. The consistency check between the HAL QCD method with the point sink operator (without LapH smearing) and the Lüscher’s finite volume method in this channel has been performed in quenched QCD [42], where the good agreement of the phase shifts between the HAL QCD method and the Lüscher’s finite volume method has been demonstrated. Thus, a purpose of this paper is to establish the sink operator independence of the scattering phase shifts in this channel even when the potential is modified due to smeared sink operators.

This paper is organized as follows. In Sec. II, we introduce the HAL QCD potential method and explain the LapH smearing scheme for the operator construction. In Sec. III, the numerical setup used in this study is explained. In Sec. IV, we calculate the potential in several different schemes, from which the scattering phase shifts are obtained. This section is the main part of this paper, where we investigate the convergence of the derivative expansion in different sink operator schemes. Sec. V is devoted to the summary of this paper. Some technical details are given in appendices.

II. THE SCHEME IN THE HAL QCD METHOD

A. Original HAL QCD method

The most important quantity in the HAL QCD method is the Nambu-Bethe-Salpeter (NBS) wave function, which is defined for the $I = 2$ $\pi\pi$ system as

$$\psi_{n_s}^{W_k}(\mathbf{r}) = \sum_{\mathbf{x}} \langle 0 | \pi_{n_s}^-(\mathbf{x}, 0) \pi_{n_s}^-(\mathbf{x} + \mathbf{r}, 0) | \pi^- \pi^-, W_k \rangle, \quad (1)$$

where $|0\rangle$ is the QCD vacuum, $|\pi^- \pi^-, W_k\rangle$ is the $\pi\pi$ eigenstate in the $(I, I_z) = (2, -2)$ channel, $W_k = 2\sqrt{m_\pi^2 + k^2}$ is the central mass energy with the momentum \mathbf{k} and its magnitude $k \equiv |\mathbf{k}|$, and $\pi_{n_s}^-(x)$ is the negatively charged pion operator, defined by

$$\pi_{n_s}^-(x) = \sum_a \bar{u}_{n_s}^a(x) \gamma_5 d_{n_s}^a(x), \quad (2)$$

where a is the index for color, and the label n_s represents the smearing level, which will be explained in the later subsection. The crucial property of the NBS wave function (below inelastic threshold $W_{\text{th}} = 4m_\pi$) is that the phase shift $\delta(k)$ is encoded in the asymptotic behaviors of $\psi_{n_s}^{W_k}(\mathbf{r})$ [16, 18, 19].

The non-local but energy-independent potential is defined from the NBS wave function as

$$\left[\frac{k^2}{m_\pi} - H_0 \right] \psi_{n_s}^{W_k}(\mathbf{r}) = \int d^3r' U_{n_s}(\mathbf{r}, \mathbf{r}') \psi_{n_s}^{W_k}(\mathbf{r}'), \quad (W_k < W_{\text{th}}) \quad (3)$$

where $H_0 \equiv -\nabla^2/m_\pi$, and m_π is the pion mass. The potential $U_{n_s}(\mathbf{r}, \mathbf{r}')$ is faithful to the phase shift below inelastic threshold, while $U_{n_s}(\mathbf{r}, \mathbf{r}')$ itself is not a physical observable and explicitly depends on the definition of the pion operator in NBS wave function, such as the smearing level n_s .

B. Time-dependent HAL QCD method

In this subsection, we explain the time-dependent HAL QCD method [17], which we employ to extract the potential reliably.

We denote the 2-pt correlation functions as

$$\mathcal{C}_{n_a, n_b}^2(t, t_0) = \sum_{\mathbf{x}, \mathbf{y}} \langle \pi_{n_a}^-(\mathbf{x}, t) \pi_{n_b}^+(\mathbf{y}, t_0) \rangle, \quad (4)$$

where n_a (n_b) is the smearing level of the sink (source) operator, and $\pi^- = \bar{u}\gamma_5 d$, $\pi^+ = \bar{d}\gamma_5 u$. The potentials are extracted from the 4-pt correlation function with various combinations of n_a and n_b , which is given by

$$\mathcal{C}_{n_a, n_b}^{4, A_1^+, 1}(\mathbf{r}, t; |\mathbf{P}|, t_0) = \sum_{\mathbf{x}} \left\langle \pi_{n_a}^-(\mathbf{x}, t) \pi_{n_a}^-(\mathbf{x} + \mathbf{r}, t) (\pi_{n_b} \pi_{n_b})_{2,2}^{A_1^+, 1}(|\mathbf{P}|, t_0) \right\rangle, \quad (5)$$

with

$$(\pi_{n_s} \pi_{n_s})_{I, I_z}^{\Lambda, \mu}(|\mathbf{P}|, t) = \sum_{\substack{\mathbf{P} \\ |\mathbf{P}|: \text{fix}}} \sum_{I_1, I_2} \sum_{\mathbf{x}, \mathbf{y}} C^{\Lambda, \mu}(\mathbf{P}) D_{I_1, I_2}^{I, I_z} e^{-i\mathbf{P} \cdot \mathbf{x}} e^{i\mathbf{P} \cdot \mathbf{y}} \pi_{n_s}^{I_1}(\mathbf{x}, t) \pi_{n_s}^{I_2}(\mathbf{y}, t), \quad (6)$$

where $C^{\Lambda, \mu}(\mathbf{P})$ is the Clebsch-Gordan coefficients in the μ -th component of the irreducible representation Λ of the cubic group, and the relative momentum \mathbf{P} is an element of $\{g\mathbf{P}_0 \mid g \in O_h, \mathbf{P}_0 = [n, 0, 0] \text{ in lattice unit with } |\mathbf{P}_0| \leq 2\}$, while D_{I_1, I_2}^{I, I_z} is that from two pions with the z component of the isospin I_1 and I_2 to the two pion system with the total isospin I and its z component I_z . Hereafter we exclusively take $\Lambda = A_1^+$ and $\mu = 1$.

The 4-pt correlation function in Eq. (5) can be decomposed into a product of the NBS wave function $\psi_{n_a}^{W_k}(\mathbf{r})$ and the time-dependent part for each eigenstate as

$$\mathcal{C}_{n_a, n_b}^{4, A_1^+, 1}(\mathbf{r}, t; |\mathbf{P}|, t_0) = \sum_k A_{n_b}^{W_k} \psi_{n_a}^{W_k}(\mathbf{r}) e^{-W_k(t-t_0)} + \dots, \quad (7)$$

where $A_{n_b}^{W_k} \equiv \left\langle \pi^- \pi^-, W_k \left| (\pi_{n_b} \pi_{n_b})_{2,2}^{A_1^+, 1}(|\mathbf{P}|, 0) \right| 0 \right\rangle$ is the overlap between the QCD eigenstate and the vacuum with the insertion of a two-pion operator, and the ellipsis represents inelastic contributions, which become negligible at moderately large $t - t_0$ and thus will be neglected in further discussions. Here indices for the irreducible representation and the isospin are omitted in $A_{n_b}^{W_k}$ for simplicity.

The R-correlator, defined by

$$R_{n_a, n_b}^{A_1^+, 1}(\mathbf{r}, t; |\mathbf{P}|, t_0) \equiv \mathcal{C}_{n_a, n_b}^{4, A_1^+, 1}(\mathbf{r}, t; |\mathbf{P}|, t_0) / \{\mathcal{C}_{n_a, n_b}^2(t, t_0)\}^2, \quad (8)$$

satisfies

$$\left(\frac{1}{4m_\pi} \frac{\partial^2}{\partial t^2} - \frac{\partial}{\partial t} - H_0 \right) R_{n_a, n_b}^{A_1^+, 1}(\mathbf{r}, t; |\mathbf{P}|, t_0) = \int d^3 r' U_{n_a}(\mathbf{r}, \mathbf{r}') R_{n_a, n_b}^{A_1^+, 1}(\mathbf{r}', t; |\mathbf{P}|, t_0), \quad (9)$$

where the scheme dependence of the potential on the sink operator is explicit as U_{n_a} [17]. It is essential that all elastic states can be used to extract the non-local potential $U_{n_a}(\mathbf{r}, \mathbf{r}')$, and the ground state saturation is not required any more in this method. We note that, by

construction, $U_{n_a}(\mathbf{r}, \mathbf{r}')$ does not depend on quantities in the source operator such as the relative momentum $|\mathbf{P}|$ and the source smearing level n_b .

In practice, we approximate the non-local potential $U_{n_a}(\mathbf{r}, \mathbf{r}')$ by the first few orders of the derivative expansion as

$$U_{n_a}(\mathbf{r}, \mathbf{r}') = \{V_{n_a}^{(0)}(r) + V_{n_a}^{(1)}(r)\nabla^2 + \mathcal{O}(\nabla^4)\} \delta^{(3)}(\mathbf{r} - \mathbf{r}'). \quad (10)$$

In this paper, we extract the potentials in the next-to-leading order (NLO) decomposition, $V_{n_a}^{(0)}(r)$ and $V_{n_a}^{(1)}(r)$, by combining R-correlators with $|\mathbf{P}| = 0, 1$, neglecting $\mathcal{O}(\nabla^4)$ terms, as explained in the next section. We also define the (effective) leading order (LO) potential given by

$$\begin{aligned} V_{n_a}^{\text{LO}}(r; |\mathbf{P}|, n_b) &\equiv \frac{\left(\frac{1}{4m_\pi} \frac{\partial^2}{\partial t^2} - \frac{\partial}{\partial t} - H_0\right) R_{n_a, n_b}^{A_1^+, 1}(\mathbf{r}, t; |\mathbf{P}|, t_0)}{R_{n_a, n_b}^{A_1^+, 1}(\mathbf{r}, t; |\mathbf{P}|, t_0)} \\ &= V_{n_a}^{(0)}(r) + V_{n_a}^{(1)}(r) \frac{\nabla^2 R_{n_a, n_b}^{A_1^+, 1}(\mathbf{r}, t; |\mathbf{P}|, t_0)}{R_{n_a, n_b}^{A_1^+, 1}(\mathbf{r}, t; |\mathbf{P}|, t_0)}, \end{aligned} \quad (11)$$

where we make relative momentum ($|\mathbf{P}|$) and source operator (n_b) dependence, introduced by the second term, explicit as $V_{n_a}^{\text{LO}}(r; |\mathbf{P}|, n_b)$. Thus, if $V_{n_a}^{\text{LO}}(r, |\mathbf{P}|, n_b)$ does not strongly depend on $|\mathbf{P}|$ or n_b , we can conclude that

$$V_{n_a}^{(1)}(r) \frac{\nabla^2 R_{n_a, n_b}^{A_1^+, 1}(\mathbf{r}, t; |\mathbf{P}|, t_0)}{R_{n_a, n_b}^{A_1^+, 1}(\mathbf{r}, t; |\mathbf{P}|, t_0)} \quad (12)$$

is small, so that $V_{n_a}^{\text{LO}}(r; |\mathbf{P}|, n_b) (\simeq V_{n_a}^{(0)}(r))$ can be used to calculate the scattering phase shifts reliably around the energies probed by the R-correlators.

C. Phase shift

Once the local potentials $V_{n_a}^{(i)}(r)$ are obtained, the scattering phase shifts can be calculated by solving the Schrödinger equation, Eq. (3). As noted before, the phase shifts should be independent of the sink operator scheme (n_a) as long as a sufficient number of local potentials $V_{n_a}^{(i)}$ ($i = 0, 1, \dots$) are employed to represent the non-local potential, though each term $V_{n_a}^{(i)}$ might have sizable dependence on the sink operator scheme [19].

In this paper, we check this scheme independence of the $I = 2$ $\pi\pi$ scattering phase shifts at the NLO level. As it has already been shown [42] and is confirmed in this paper

(Sec. IV A), the contribution from NLO or higher order terms to the potential in the point-sink scheme is negligibly small in this channel, so that the effective LO potential gives the correct phase shifts below a certain energy. Therefore, we can use the scattering phase shifts from the potential in the point-sink scheme as the benchmark of our analysis. We compare the scattering phase shifts calculated from the potentials in the LapH smearing scheme with the benchmark, in order to see how good the NLO analysis in the derivative expansion is in this scheme.

D. Some remarks and comments on Ref. [43]

As already stressed many times before [16, 18, 19], the quantitative comparison between different schemes can be done only through physical observables but not through potentials. The comparison between potentials is analogous to the comparison of the running couplings among different schemes such as $\alpha_{\overline{\text{MS}}}(q)$ ($\overline{\text{MS}}$ scheme), $\alpha_V(q)$ (potential scheme) or $\alpha_{\text{SF}}(q)$ (Shrödinger functional scheme) in QCD. We must compare physical quantities such as the scattering phase shifts in the case of the potential or the scattering amplitudes in the case of the running coupling. Although physical observables are scheme independent in principle, approximations introduced to calculate them bring the scheme dependence into observables. An example for the approximations is the truncation of the derivative expansion for the potential or that of the perturbative expansion for the running coupling. In such cases, one scheme is better than others for the fast convergence of the approximation. In the case of the potential, the point-sink scheme is shown to be a good scheme for the fast convergence of the derivative expansion [23, 42], so that even the local potential at the LO gives reasonable results at low energies. Analogous scheme dependence for the convergence of the perturbative expansion exist for the running coupling.

Here we make a few comments on a recent paper [43] whose discussions are trivially invalidated as shown below.

The first point discussed in [43] is the relation between the (local) energy-dependent potential and phase shifts, where it was claimed that the energy-dependent potential defined at a given energy can give the correct phase shift only at that energy, but gives incorrect phase shifts at different energies. We note that such a claim is nothing to do with the HAL QCD method, since the theoretical formulation of the HAL QCD method is based on not the

energy-dependent potential, but the non-local energy-independent potential $U(\mathbf{r}, \mathbf{r}')$, where it was proven that the latter is faithful to the phase shifts at all energies below the inelastic threshold [16, 18, 19]. As discussed above as well as in our previous papers [16, 18, 19], the derivative expansion for the non-local potential, so far employed in our applications, gives some truncation errors at given orders of the expansion, which however should not be misunderstood as the theoretical limitation of the HAL QCD method.

The second point discussed in Ref. [43] is the derivative expansion of the non-local potential $U(\mathbf{r}, \mathbf{r}')$. We first note that the information of $\psi_{n_s}^{W_k}(\mathbf{r})$ (in particular the phase shifts $\delta(k)$) below the inelastic threshold are encoded in $U(\mathbf{r}, \mathbf{r}')$, where the degrees of freedom of \mathbf{r} and \mathbf{k} in the former are implicitly converted to those of \mathbf{r} and \mathbf{r}' in the latter through Eq. (3). The derivative expansion of the non-local potential is given by

$$U(\mathbf{r}, \mathbf{r}') = \sum_{\mathbf{n}} V_{\mathbf{n}}(\mathbf{r}) \nabla_{\mathbf{r}}^{\mathbf{n}} \delta^{(3)}(\mathbf{r} - \mathbf{r}'), \quad \nabla_{\mathbf{r}}^{\mathbf{n}} \equiv \nabla_{r_x}^{n_x} \nabla_{r_y}^{n_y} \nabla_{r_z}^{n_z}, \quad (13)$$

where no symmetry is assumed. Ref. [43] claimed that $V_{\mathbf{n}}(\mathbf{r})$ cannot be \mathbf{k} independent since $U(\mathbf{r}, \mathbf{r}')$ needs the same number of the degrees of freedom, \mathbf{r} and \mathbf{r}' , to keep the \mathbf{k} independence of $U(\mathbf{r}, \mathbf{r}')$. Clearly this statement is incorrect since \mathbf{n} has enough degrees of freedom to describe \mathbf{r}' dependence. For instance, using the Taylor expansion as

$$\begin{aligned} \int d^3 r' U(\mathbf{r}, \mathbf{r}') \psi(\mathbf{r}'; \mathbf{k}) &= \sum_{\mathbf{n}} \int d^3 r' U(\mathbf{r}, \mathbf{r}') \frac{(\mathbf{r}' - \mathbf{r})^{\mathbf{n}}}{\mathbf{n}!} \nabla_{\mathbf{r}}^{\mathbf{n}} \psi(\mathbf{r}; \mathbf{k}), \\ \frac{(\mathbf{r}' - \mathbf{r})^{\mathbf{n}}}{\mathbf{n}!} &\equiv \frac{(r'_x - r_x)^{n_x}}{n_x!} \frac{(r'_y - r_y)^{n_y}}{n_y!} \frac{(r'_z - r_z)^{n_z}}{n_z!}, \end{aligned} \quad (14)$$

we can express $V_{\mathbf{n}}(\mathbf{r})$ in terms of $U(\mathbf{r}, \mathbf{r}')$ as

$$V_{\mathbf{n}}(\mathbf{r}) = \int d^3 r' U(\mathbf{r}, \mathbf{r}') \frac{(\mathbf{r}' - \mathbf{r})^{\mathbf{n}}}{\mathbf{n}!}, \quad (15)$$

which are manifestly \mathbf{k} independent.

The third point discussed in Ref. [43] is a relation between the scattering phase shift and the smearing of operator. Ref. [43] considered the following relation (Eq. (11) in Ref. [43] and called the “fundamental relation” in that paper)

$$-\int d^3 r h(r; k) e^{-i\mathbf{k} \cdot \mathbf{r}} = \frac{4\pi}{k} e^{i\delta_0(k)} \sin \delta_0(k), \quad h(r; k) \equiv (\nabla^2 + k^2) \psi_0(r; k), \quad (16)$$

where $\delta_0(k)$ is the S-wave scattering phase shift and ψ_0 is the S-wave NBS wave function.

One can further consider the smeared NBS wave function defined by

$$\tilde{\psi}_0(r; k) = \int d^3 r' s(|\mathbf{r} - \mathbf{r}'|) \psi_0(r'; k), \quad \tilde{h}(r; k) \equiv (\nabla^2 + k^2) \tilde{\psi}_0(r; k), \quad (17)$$

with $s(r)$ is a smearing function. In Ref. [43], it was claimed that the “fundamental relation” does not hold by this smearing as (Eq. (26) in Ref. [43])

$$-\int d^3r \tilde{h}(r; k) e^{-i\mathbf{k}\cdot\mathbf{r}} = -\int d^3r \int d^3r' s(|\mathbf{r}-\mathbf{r}'|) h(r'; k) e^{-i\mathbf{k}\cdot\mathbf{r}} \neq \frac{4\pi}{k} e^{i\delta_0(k)} \sin \delta_0(k), \quad (18)$$

and the correct phase shift $\delta_0(k)$ is not obtained from the smeared NBS wave function, Eq. (17). This claim is also incorrect. Using $\mathbf{k} \cdot \mathbf{r} = \mathbf{k} \cdot (\mathbf{r} - \mathbf{r}') + \mathbf{k} \cdot \mathbf{r}'$, we have

$$-\int d^3r \tilde{h}(r; k) e^{-i\mathbf{k}\cdot\mathbf{r}} = -C(k) \int d^3r' h(r'; k) e^{-i\mathbf{k}\cdot\mathbf{r}'} = C(k) \frac{4\pi}{k} e^{i\delta_0(k)} \sin \delta_0(k), \quad (19)$$

$$C(k) \equiv \int d^3r s(|\mathbf{r}|) e^{-i\mathbf{k}\cdot\mathbf{r}}, \quad (20)$$

so that the “fundamental relation” is satisfied if we use $\tilde{h}(r; k)/C(k)$ instead of $\tilde{h}(r; k)$. This normalization is indeed necessary and correct since $\psi_0(r; k) = j_0(kr) + \text{scattering wave}$ implies $\tilde{\psi}_0(r; k) = C(k)(j_0(kr) + \text{scattering wave})$.

E. LapH smearing

The smeared pion operator at time t is constructed as

$$\pi_{n_s}^{fg}(\mathbf{x}, t) = \sum_a \bar{q}_{n_s}^{a,f}(\mathbf{x}, t) \gamma_5 q_{n_s}^{a,g}(\mathbf{x}, t) \quad (21)$$

from the smeared quark operator given by

$$q_{n_s}^{a,f}(\mathbf{x}, t) = \sum_{b,\mathbf{y}} \mathcal{S}_{n_s}^{ab}(\mathbf{x}, \mathbf{y}; t) q^{b,f}(\mathbf{y}, t), \quad (22)$$

where $q^{a,f}(\mathbf{x}, t)$ is a local quark field with a color index a and a flavor index f ($f = 1, 2$ for u, d quarks), \mathcal{S} is a smearing operator at time t with smearing level n_s [35, 36]. Note that the spinor indices of quarks are implicit and are summed over in the pion operator. Hereafter a summation over repeated indices is assumed, unless otherwise stated.

In this paper, we employ the gauge covariant smearing operator \mathcal{S} , which is constructed from a gauge covariant lattice Laplacian at t defined by

$$\tilde{\Delta}^{ab}(\mathbf{x}, \mathbf{y}, t) = \sum_{i=1}^3 \left(\tilde{U}_i^{ab}(\mathbf{x}, t) \delta_{\mathbf{x}, \mathbf{y}+\hat{i}} - 2\delta_{\mathbf{x}, \mathbf{y}} + \tilde{U}_i^{\dagger ab}(\mathbf{y}, t) \delta_{\mathbf{x}, \mathbf{y}-\hat{i}} \right),$$

where $\tilde{U}_i^{ab}(\mathbf{x}, t)$ represents a stout-smeared link variable [44]. This operator can be diagonalized as

$$\tilde{\Delta}^{ab}(\mathbf{x}, \mathbf{y}, t) = \sum_{n=1}^{n_{\max}} V_n^a(\mathbf{x}, t) \lambda_n V_n^{b\dagger}(\mathbf{y}, t), \quad (23)$$

where λ_n is the n -th eigenvalue with $|\lambda_n| \leq |\lambda_m|$ for $n < m$, $V_n^a(\mathbf{x}, t)$ is the corresponding eigenvector, and $n_{\max} = N_{\text{color}} N_x N_y N_z$. Using eigenvectors, \mathcal{S} with the smearing level n_s is given by

$$\mathcal{S}_{n_s}^{ab}(\mathbf{x}, \mathbf{y}; t) = \sum_{n=1}^{n_s} V_n^a(\mathbf{x}, t) V_n^{b\dagger}(\mathbf{y}, t), \quad (24)$$

which is the projection operator to the space spanned by n_s eigenvectors. We call this smearing the LapH smearing with the level n_s . Since the eigenmodes corresponding to larger values of $|\lambda_n|$ are absent in this subspace, the smearing operator \mathcal{S} removes high momentum components of quark fields in a gauge covariant manner. Roughly speaking, $n_s = 8, 16, 32$ and 64 in our setup correspond to the momentum cutoff of 680 MeV, 770 MeV, 900 MeV and 1100 MeV, respectively. Note that the point quark with no smearing is given by $n_s = n_{\max}$. We also study the wall quark operator (only at the source), for which we use the short-hand notation “ $n_s = 0$ ” even though it does not belong to the LapH smearing.

III. NUMERICAL SETUP

Since the main purpose of this paper is to investigate the scheme independence of the scattering phase shifts, we perform a lattice QCD calculation at a single heavy pion mass on a small lattice. We employ the $2 + 1$ flavor gauge configuration on a $16^3 \times 32$ lattice, generated by JLQCD and CP-PACS collaborations with a renormalization-group improved gauge action at $\beta = 1.83$ and non-perturbatively improved clover action with $c_{SW} = 1.7610$ at the hopping parameters $k_{ud} = 0.1376$ and $k_s = 0.1371$ [45, 46]. These parameters correspond to the lattice spacing $a \simeq 0.1214$ fm ($a^{-1} \simeq 1.625$ GeV), so that the physical lattice size is $L^3 \times T \simeq (1.94 \text{ fm})^3 \times 3.88 \text{ fm}$, and the pion mass $m_\pi \simeq 870$ MeV. The stout-smearing parameters for the link variables in the gauge covariant Laplacian operator are chosen as staple weight $\rho = 0.1$ and iteration number $n_\rho = 10$. For the calculation of the NBS wave function, the periodic boundary condition is employed in all directions, except for the point sink and smeared/wall source combinations, where the Dirichlet boundary condition is employed in the temporal direction. In the case of the Dirichlet boundary condition, the source is located at the midpoint of the temporal direction. In the case of the wall source, the Coulomb gauge fixing is employed. The number of configurations used in this paper is 60

for all the sink-source combinations except for the point sink and wall source combination, where 700 configurations are used, and we calculate with 32 different source time slices per configuration. We take $t - t_0 = 11$ for all cases, except $t - t_0 = 12$ for $n_a = n_b = 16$ case and the point-sink cases, where the single pion 2-pt function is saturated by the ground state.

IV. RESULTS

A. Potentials and scattering phase shifts in the point-sink scheme

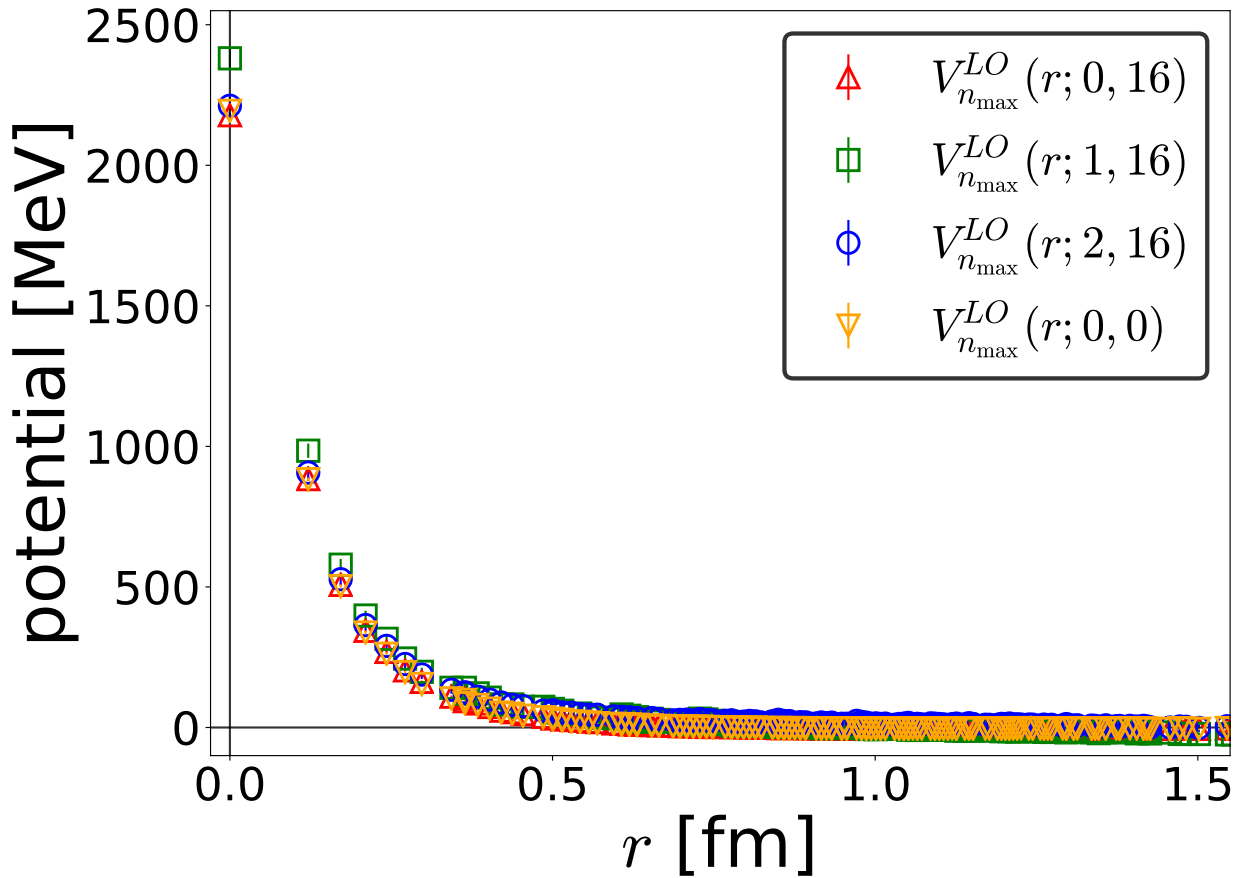


FIG. 1: The effective LO potentials in the point-sink scheme $V_{n_{\max}}^{\text{LO}}(r; |\mathbf{P}|, n_b)$ with $n_b = 16$ at $|\mathbf{P}| = 0$ (red up triangles), 1 (green squares), 2 (blue circles), together with $V_{n_{\max}}^{\text{LO}}(r; 0, n_b)$ with $n_b = 0$ (orange down triangles).

We first study the point-sink scheme. In Fig. 1, we show the effective LO potentials in the point-sink scheme, $V_{n_{\max}}^{\text{LO}}(r; |\mathbf{P}|, 16)$ with $|\mathbf{P}| = 0$ (red up triangles), 1 (green squares), 2 (blue

circles), together with the one calculated from the wall source, $V_{n_{\max}}^{\text{LO}}(r; |\mathbf{P}| = 0, 0)$ (orange down triangles). The temporal separation, $t - t_0 = 12$, is large enough for the potential to be stable against the change of $t - t_0$. We first notice that the source operator dependence, the difference between the smeared with $n_b = 16$ and the wall source is negligible, by comparing $V_{n_{\max}}^{\text{LO}}(r; |\mathbf{P}| = 0, 16)$ (red up triangles) and $V_{n_{\max}}^{\text{LO}}(r; |\mathbf{P}| = 0, 0)$ (orange down triangles). In addition, it is observed that $V_{n_{\max}}^{\text{LO}}(r; |\mathbf{P}|, 16)$ is almost independent of the source momentum $|\mathbf{P}| \leq 2$.

We obtain the scattering phase shifts by solving the Schrödinger equation with the potentials which are fit by the following functional form,

$$V^{\text{LO}}(r) = A_1 e^{-\frac{r^2}{\sigma_1^2}} + A_2 e^{-\frac{r^2}{\sigma_2^2}}. \quad (25)$$

The fit of potential works well for $|\mathbf{P}| = 0$ and 2, while there exist some residual errors for $|\mathbf{P}| = 1$, since $V_{n_{\max}}^{\text{LO}}(r; |\mathbf{P}| = 1, 16)$ at large r slightly deviates from zero. This introduces systematic uncertainties in results from $|\mathbf{P}| = 1$, as discussed later.

Shown in Fig. 2 are the obtained phase shifts in terms of k^2 , where we compare the results from $V_{n_{\max}}^{\text{LO}}(r; |\mathbf{P}|, 16)$ between $|\mathbf{P}| = 0$ and 1 (upper panel) and between $|\mathbf{P}| = 0$ and 2 (lower panel), where the bands correspond to the statistical errors only. The phase shifts from $V_{n_{\max}}^{\text{LO}}(r; |\mathbf{P}| = 0, 0)$ are almost identical to those from $V_{n_{\max}}^{\text{LO}}(r; |\mathbf{P}| = 0, 16)$, and are not shown in the figure. The most important observation in Fig. 2 is that, at low energies, the phase shifts are independent of the source within statistical errors and the effective LO potential in the point-sink scheme describes the $I = 2$ $\pi\pi$ scattering rather precisely. We thus confirm that the conclusion of the previous quenched study for the $I = 2$ $\pi\pi$ scattering [42] that the potential in the point-sink scheme, the standard for the HAL QCD potential, is a good scheme also in the full QCD, so that the effective LO potential gives a reliable approximation for the non-local potential up to a certain energy. In order to estimate the energy above which NLO corrections would affect the results, we look at Fig. 2 in more details. In the upper panel, we find that the results from $|\mathbf{P}| = 0$ (red) and $|\mathbf{P}| = 1$ (green) are consistent with each other at least up to $k^2 \lesssim 0.4 \text{ GeV}^2$. As discussed above, the results from $|\mathbf{P}| = 1$ would suffer from additional systematic errors, and thus the results from $|\mathbf{P}| = 0$ and 1 may be consistent even at higher energies. In the lower panel, we find that the results from $|\mathbf{P}| = 0$ (red) and $|\mathbf{P}| = 2$ (blue) are consistent with each other at least up to $k^2 \lesssim 0.6 \text{ GeV}^2$. As a conservative estimate, we conclude that effective LO analysis

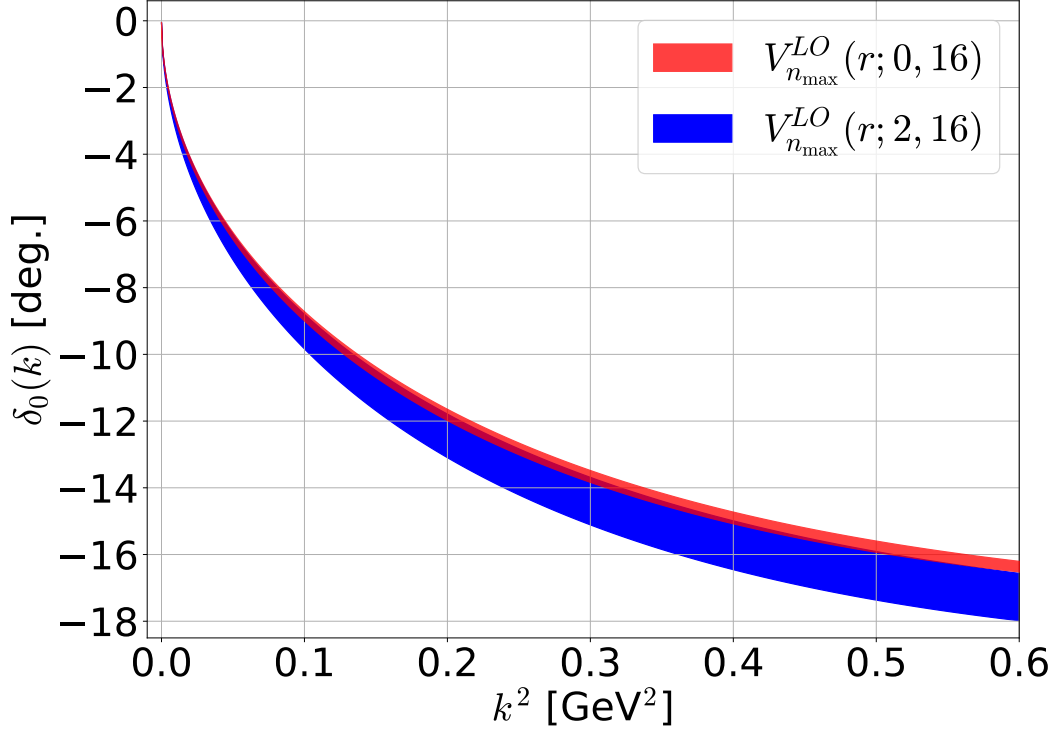
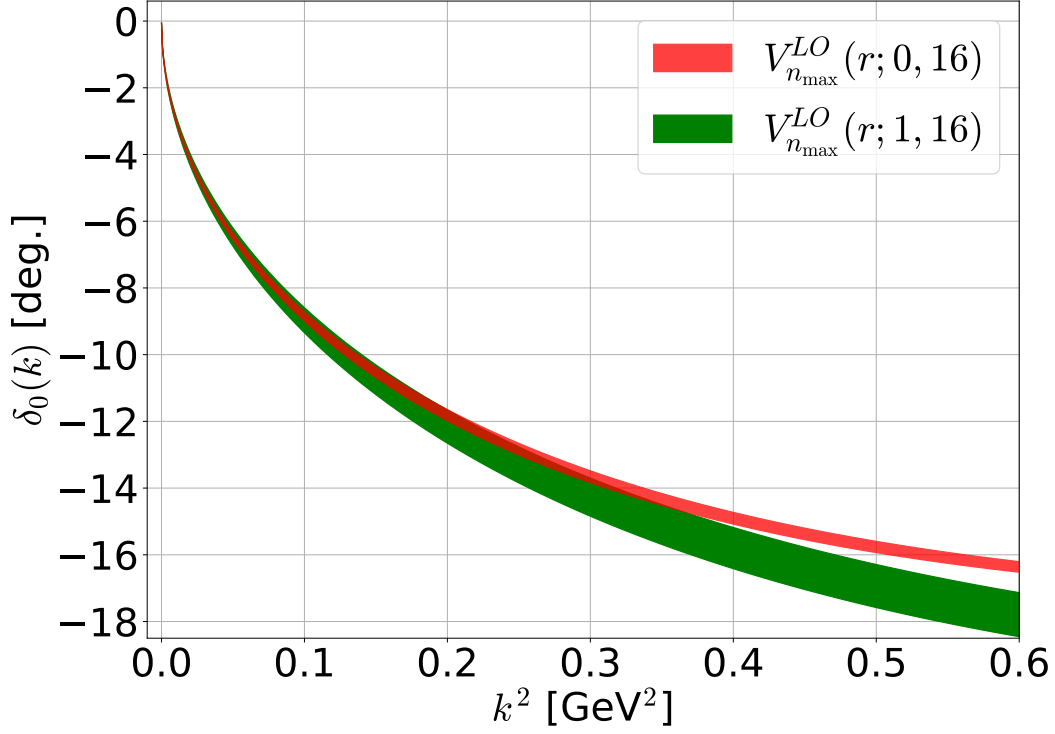


FIG. 2: The phase shifts of the S-wave $I = 2$ $\pi\pi$ scattering in the point-sink scheme $V_{n_{\max}}^{\text{LO}}(r; |\mathbf{P}|, 16)$. (Upper) The results from $|\mathbf{P}| = 0$ (red) and $|\mathbf{P}| = 1$ (green) are compared. (Lower) The results from $|\mathbf{P}| = 0$ (red) and $|\mathbf{P}| = 2$ (blue) are compared.

in the point-sink scheme is reliable, at least up to $k^2 \lesssim 0.4 \text{ GeV}^2$. Among the results in the point-sink scheme, those from $|\mathbf{P}| = 0$ give the smallest statistical fluctuations, and we therefore use the scattering phase shifts from $V_{m_{\max}}^{\text{LO}}(r; |\mathbf{P}| = 0, 16)$ as the benchmark in our investigation hereafter.

B. Potentials in the smeared-sink scheme

We now consider the potential in the smeared-sink scheme. Fig. 3 shows the effective LO potentials in the smeared-sink scheme with $n_a = 64$ from the smeared source with $n_b = 64$, $|\mathbf{P}| = 0, 1$, obtained at $t - t_0 = 11$. It turns out that potentials have sizable source momentum dependence unlike the case of the point-sink scheme. It is also found that the potentials have non-negligible dependence on $t - t_0$ for $|\mathbf{P}| = 1$. These observations indicate that the NLO contribution cannot be neglected in this scheme. We therefore determine $V^{(0)}$ and $V^{(1)}$ separately, by solving

$$\begin{pmatrix} 1 & \frac{\nabla^2 R_{n_a, n_b}^{A_1^+, 1}(\mathbf{r}, t; 0, t_0)}{R_{n_a, n_b}^{A_1^+, 1}(\mathbf{r}, t; 0, t_0)} \\ 1 & \frac{\nabla^2 R_{n_a, n_b}^{A_1^+, 1}(\mathbf{r}, t; 1, t_0)}{R_{n_a, n_b}^{A_1^+, 1}(\mathbf{r}, t; 1, t_0)} \end{pmatrix} \begin{pmatrix} V_{n_a}^{(0)}(r) \\ V_{n_a}^{(1)}(r) \end{pmatrix} = \begin{pmatrix} V_{n_a}^{\text{LO}}(r; 0, n_b) \\ V_{n_a}^{\text{LO}}(r; 1, n_b) \end{pmatrix}. \quad (26)$$

Fig. 4 shows $V_{64}^{(0)}(r)$ (green up triangles) and $m_\pi^2 V_{64}^{(1)}(r)$ (orange diamonds), together with $V_{64}^{\text{LO}}(r; 0, 64)$ (red squares) and $V_{64}^{\text{LO}}(r; 1, 64)$ (blue circles). One first notices $V_{64}^{(0)}(r) \simeq V_{64}^{\text{LO}}(r; 0, 64)$, which suggests $V_{64}^{(1)}(r) \nabla^2 R_{64, 64}^{A_1^+, 0}(\mathbf{r}, t; 0, t_0)$ is negligibly small. This means that nonzero momentum components in $R_{64, 64}^{A_1^+, 0}(\mathbf{r}, t; 0, t_0)$ is tiny. On the other hand, $R_{64, 64}^{A_1^+, 0}(\mathbf{r}, t; 1, t_0)$ contains non-zero momentum component enough to determine $V_{64}^{(0)}(r)$ and $V_{64}^{(1)}(r)$ separately, the latter of which is responsible for the difference between $V_{64}^{\text{LO}}(r; 0, 64)$ and $V_{64}^{\text{LO}}(r; 1, 64)$ in Fig. 3.

C. Scattering phase shifts in the smeared-sink scheme

We obtain the scattering phase shifts by solving the Schrödinger equation with the potential including the NLO term. For the NLO analysis, $V_{n_a}^{(0)}(r)$ is fitted with the form

$$V^{(0)}(r) = A_1 e^{-\frac{r^2}{\sigma_1^2}} + A_2 e^{-\frac{r^2}{\sigma_2^2}} \quad (27)$$

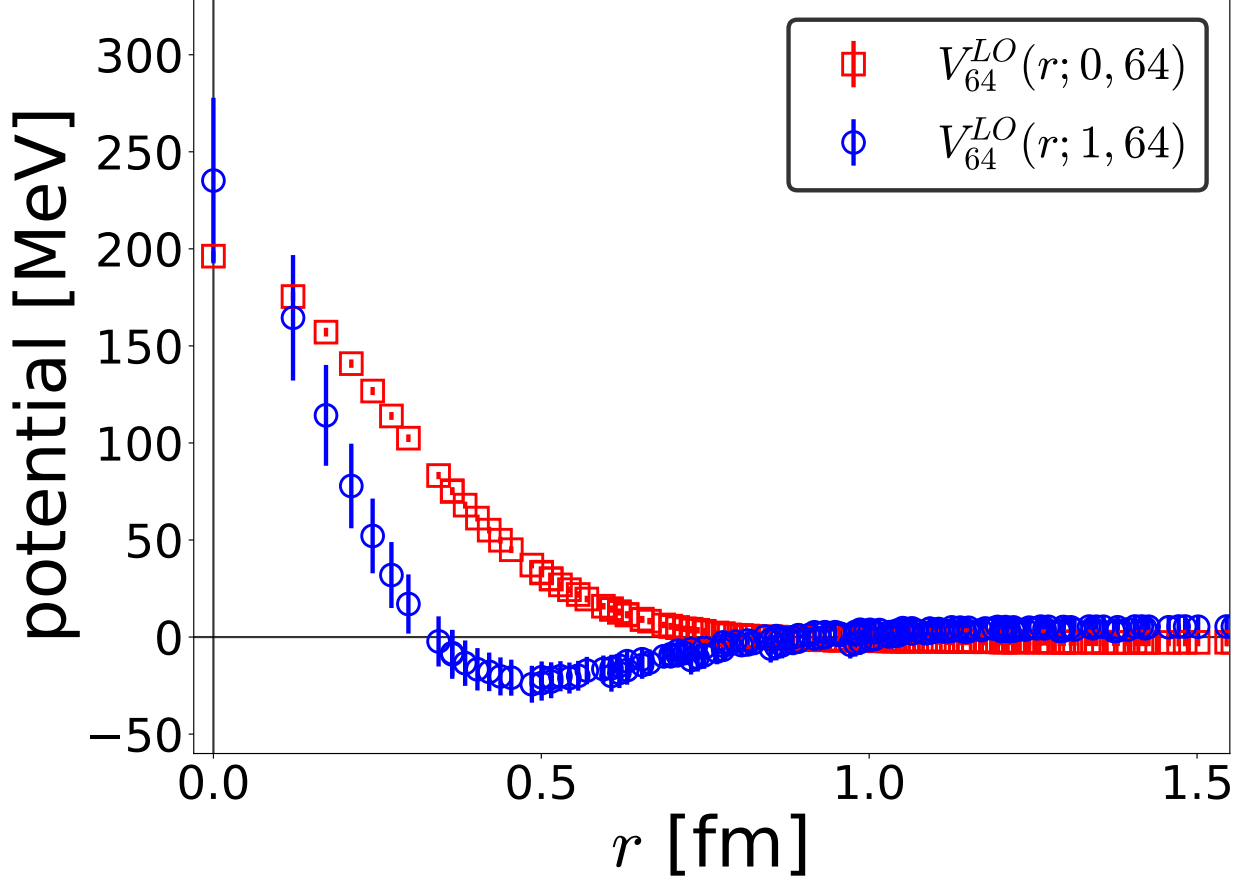


FIG. 3: The effective LO potential from the smeared-sink scheme $V_{64}^{LO}(r; |\mathbf{P}|, 64)$ at $|\mathbf{P}| = 0, 1$.

for all r , while $V_{n_a}^{(1)}(r)$ is fitted with

$$V^{(1)}(r) = A_3 e^{-\frac{r^2}{\sigma_3^2}} + A_4 e^{-\frac{(r-a)^2}{\sigma_4^2}} \quad (28)$$

for $0 \leq r \leq 0.8$ fm, which is chosen so as to exclude singular behaviors of $V_{n_a}^{(1)}(r)$ at large r in the fit. In Fig. 4, fitted functions for $V^{(0)}(r)$ and $V^{(1)}(r)$ are also given by light-blue and yellow bands, respectively.

In order to see an effect of the NLO correction on the scattering phase shifts $\delta_0(k)$ quantitatively, we show the scattering phase shifts as a function of k^2 in Fig. 5, where the benchmark result from $V_{n_{\max}}^{LO}(r; 0, 16)$ (orange) in the point-sink scheme is compared with those from $V_{64}^{LO}(r; 0, 64)$ (pink) and $V_{64}^{(0)}(r) + V_{64}^{(1)}(r)\nabla^2$ (red) in the smeared-sink scheme.

Let us first compare the scattering phase shifts between the point-sink scheme (orange) and the smeared-sink scheme (pink) at the LO. While both results agree with each other at very low energies, they start deviating as the energy increases. The difference in the

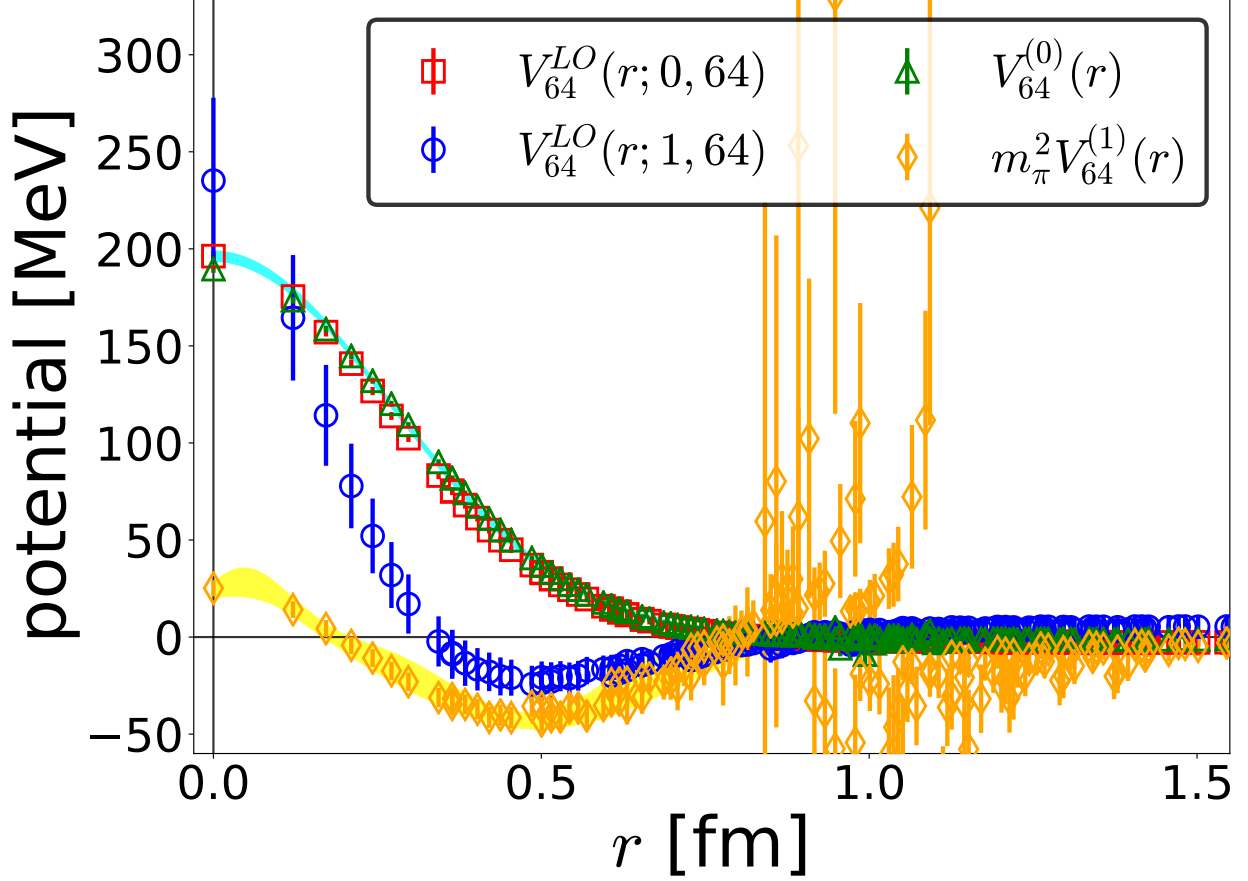


FIG. 4: The result of the NLO analysis, $V_{64}^{(0)}(r)$ (green up triangles) and $m_{\pi}^2 V_{64}^{(1)}(r)$ (orange diamonds), together with $V_{64}^{LO}(r; 0, 64)$ (red squares) and $V_{64}^{LO}(r; 1, 64)$ (blue circles) for a comparison. Light blue and yellow bands correspond to fit results of $V_{64}^{(0)}(r)$ and $V_{64}^{(1)}(r)$, respectively.

phase shift becomes about 4 degrees at $k^2 = 0.3 \text{ GeV}^2$. If the NLO analysis is employed in the smeared-sink scheme, the agreement between the point-sink scheme (orange) and the smeared-sink scheme (red) is improved as expected. The difference in the phase shift is reduced to about 2 degrees ($\simeq 15 \%$) at $k^2 = 0.3 \text{ GeV}^2$. This result indicates that the use of the NLO analysis is almost mandatory in the smeared-sink scheme for quantitatively precise descriptions of scattering phenomena by the HAL QCD potential method.

In order to see differences more precisely, $k \cot \delta_0(k)$ is plotted as a function of k^2 in Fig. 6, where the phase shifts obtained from the finite volume energy by the Lüscher's finite volume method [1] (see Appendix. B for details) are also shown at $k^2 = 7.2 \times 10^{-3}({}^{+13}_{-5})$ and $0.43({}^{+1}_{-0}) \text{ GeV}^2$ (black bands). It is clearly observed that the NLO analysis significantly improves the agreement between different schemes/methods. The results from the effective

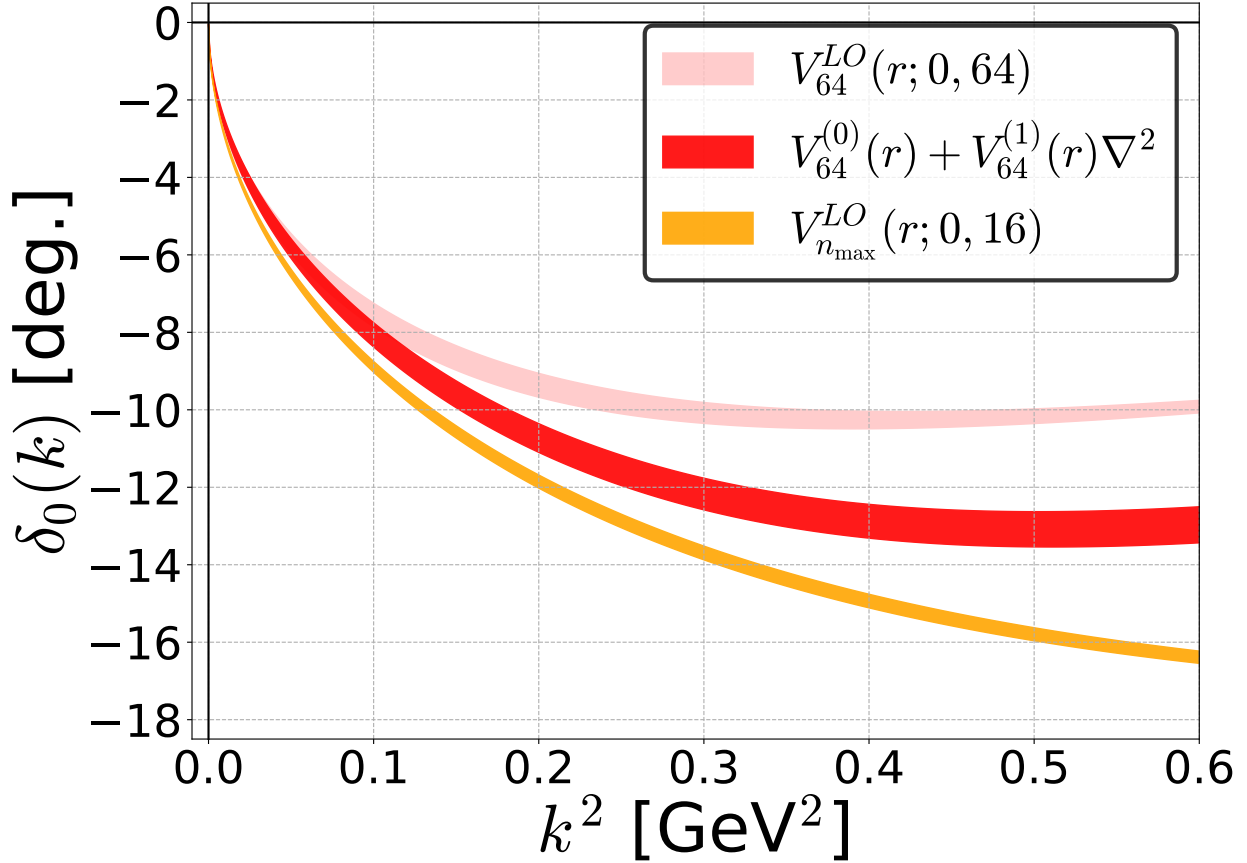


FIG. 5: The phase shifts of the S-wave $I = 2$ $\pi\pi$ scattering from the potential in the point-sink scheme (LO: orange) and the smeared-sink scheme (LO: pink, NLO: red) as a function of k^2 .

LO potential in the point-sink scheme (orange) as well as those from the NLO potentials in the smeared-sink schemes with $n_a = 64$ (red) and $n_a = 32$ (blue) agree with results from the finite volume energy shift not only at low energy ($k^2 \simeq 0$ GeV²) but also at higher energy ($k^2 \simeq 0.43$ GeV²) within their statistical errors, though statistical errors of $k \cot \delta_0(k)$ from the finite volume energy shift (black bands) are rather large. Among different schemes in the potential method, we remind readers that the results from the effective LO potential in the point-sink scheme is the most reliable as the benchmark, since the phase shifts in the point-sink scheme are robust in the sense that the source momentum dependence (the NLO term) is sufficiently small. Therefore, the difference of results between the point and smeared-sink schemes gives the remaining systematic errors in the smeared-sink scheme. The most plausible origin for this systematics at higher energies is the higher order corrections in the derivative expansion in the smeared-sink scheme. In fact, the magnitude of the remaining

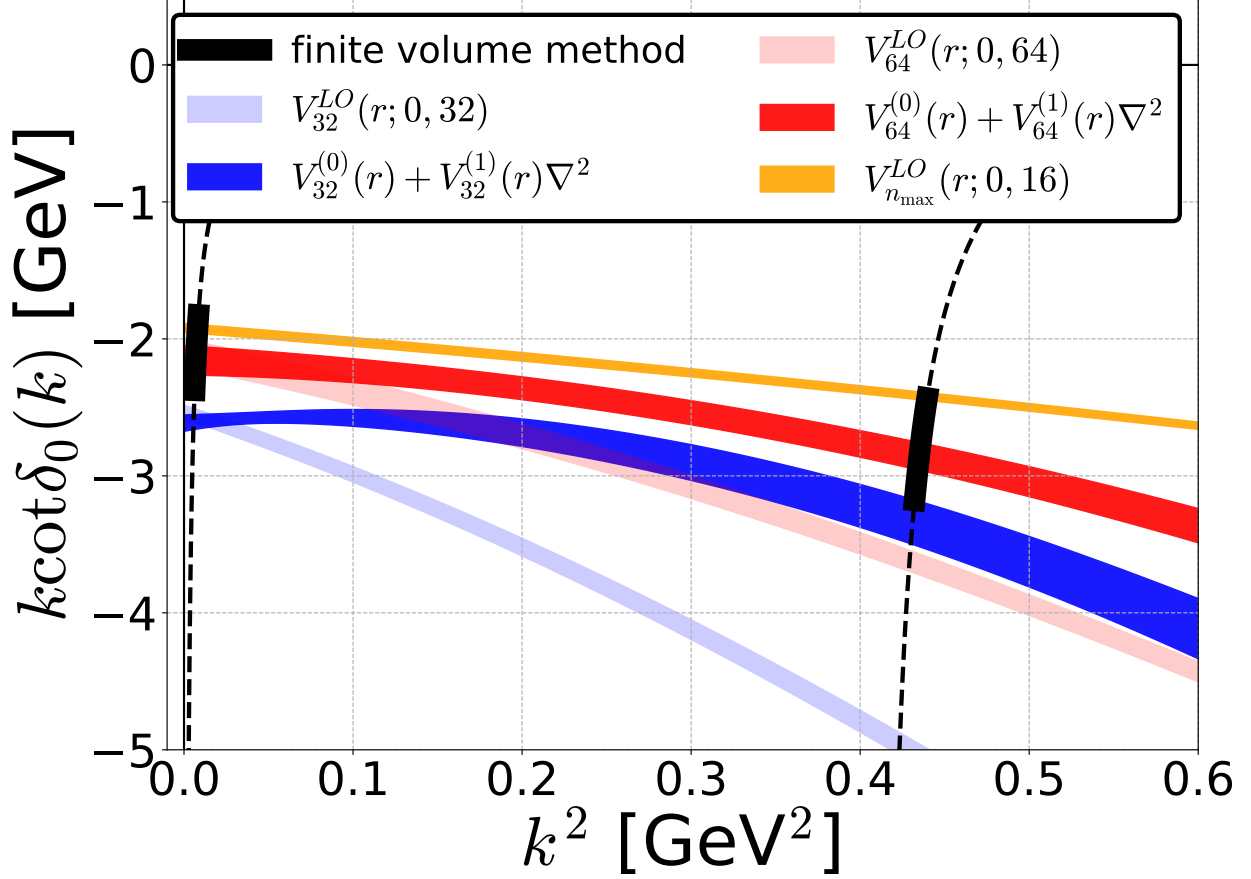


FIG. 6: $k \cot \delta_0(k)$ as a function of k^2 for the point-sink scheme (orange), the smeared-sink scheme with $n_a = n_b = 64$ (LO: pink, NLO: red) and with $n_a = n_b = 32$ (LO: light blue, NLO: blue). Black bands show the phase shift calculated from the finite volume energy shift through the Lüscher's formula, $2\mathcal{Z}_{00}(1; (\frac{kL}{2\pi})^2)/\pi^{\frac{1}{2}}L$, denoted by black dashed lines.

systematics is compatible with the magnitude of NNLO corrections which can be roughly estimated by the difference between LO and NLO results. Another possible origin is the systematics in NLO terms, since there exist uncertainties in $V^{(1)}(r)$ at long range ($r \gtrsim 0.8$ fm in Fig. 4). Note that NLO (and higher order) corrections can be reduced by increasing the smearing level n_a , as can be seen from the comparison between $n_a = 32$ and 64.

At very low energies, $k^2 \simeq 0$ GeV², while the results between different schemes/methods achieve good agreement even at the LO analysis, the inclusion of the NLO contribution does not resolve the remaining (small) deviations between the point and smeared-sink schemes. Considering that NLO correction is small and that the derivative expansion is expected to be good at low energies, higher order corrections would not be the origin of this systematics.

One of the possible reasons is the uncertainties in $V^{(1)}(r)$ at long range as mentioned above. Another possibility is the systematics associated with the long tail structure in the LapH smearing (Fig. 8), and studies to improve the locality of the LapH smearing are in progress. Again, we can reduce the systematics by increasing the smearing level n_a , as is actually seen in the figure.

In Table I, we present $k \cot \delta_0(k)$ at $k^2 = 7.2 \times 10^{-3}$ and 0.43 GeV^2 , obtained from the effective LO potential in the point-sink scheme ($n_a = n_{\text{max}}$) with $|\mathbf{P}| = 0$, as the benchmark result. We also show the LO/NLO analyses in the smeared-sink scheme with $n_a = 64$, together with results from the finite volume method, where errors are statistical only. Systematic errors in the smeared-sink scheme can be estimated by the difference between the point and smeared-sink schemes as discussed above. We then confirm that the potential method with the smeared-sink scheme and finite volume method give consistent results with similar sizes of uncertainties, which are dominated by systematic errors in the former but by statistical errors for the latter.

$k^2 \text{ (GeV}^2\text{)}$	$V_{n_{\text{max}}}^{\text{LO}}(r; 0, 16)$	$V_{64}^{\text{LO}}(r; 0, 64)$	$V_{64}^{(0)}(r) + V_{64}^{(1)}(r)\nabla^2$	finite volume method
7.2×10^{-3}	-1.94(10)	-2.13(10)	-2.17(11)	-2.11(28)
0.43	-2.42(3)	-3.65(8)	-2.86(11)	-2.83(41)

TABLE I: A comparison of $k \cot \delta_0(k)$ in units of GeV among various schemes/methods. Errors are statistical only.

V. CONCLUSION

In this paper, the scheme independence in the HAL QCD method has been investigated for the $I = 2 \pi\pi$ scattering phase shifts at $m_\pi \simeq 870 \text{ MeV}$. We have considered two schemes, the point-sink scheme and the smeared-sink scheme with various smearing levels n_a , where we newly introduce the LapH smearing in the latter. We have found in the point-sink scheme, which is the standard scheme in the HAL QCD method, that the NLO contributions are sufficiently small below $k^2 \sim 0.4 \text{ GeV}^2$. This means that the (effective) LO potential in the point-sink scheme is a good description of the $I = 2 \pi\pi$ interaction at least up to $k^2 \sim 0.4$

GeV² (2.15 GeV in terms of the central mass energy).¹ This result in full QCD confirms the conclusion in previous quenched QCD studies that the point-sink scheme is a good scheme for the HAL QCD potential for the NN system [23] and the $I = 2$ $\pi\pi$ system [42].

In the case of the smeared-sink scheme, the effective LO potential shows a sizable dependence on the momentum at the source, so that the NLO contribution is non-negligible. In fact, at the effective LO analysis, the scattering phase shifts in the smeared-sink scheme show some deviation from the benchmark result given by the point-sink scheme, which increases as the energy increases.² We thus calculated the phase shifts using the NLO analysis in the smeared sink scheme. The NLO analysis improves an agreement with the benchmark result at both low and high energies, and results in both point-sink scheme and smeared-sink scheme with $n_a = 64$ are consistent with the scattering phase shifts from the finite volume energy shift calculated by the Lüscher's formula at two energies, within large statistical errors in the finite volume method. The systematic errors of the potential method in the smearing sink scheme with $n_a = 64$ can be estimated from the difference between the point-sink scheme and the smeared-sink scheme, and are found to be similar size compared to the statistical errors of the finite volume method.

Our study in this paper gives the following lessons for future studies of resonant states such as $I = 0, 1$ $\pi\pi$ scatterings by the HAL QCD potential method in the smeared-sink scheme. (1) It is better to increase the smearing level n_a as long as computational resources (cpu time, memory, disk space, etc.) allow. (2) It is better to observe the n_a dependence carefully. (3) It is important to employ the NLO analysis if possible.

Studies of resonant states in the HAL QCD potential method are ongoing. Results will be reported in near future.

VI. ACKNOWLEDGEMENT

This work is supported in part by the Grant-in-Aid of the Japanese Ministry of Education, Sciences and Technology, Sports and Culture (MEXT) for Scientific Research (No. JP16H03978, (C)26400281, JP15K17667), by a priority issue (Elucidation of the fun-

¹ Note that the threshold of 4 π in the final state corresponds to $k = \sqrt{3}m_\pi \simeq 1.5$ GeV.

² In Appendix C, we present the effective LO analysis in the smeared-sink scheme with various smearing levels n_a .

damental laws and evolution of the universe) to be tackled by using Post “K” Computer, and by Joint Institute for Computational Fundamental Science (JICFuS). D.K. is supported in part by the Japan Society for the Promotion of Science (JSPS). T.D. is supported in part by RIKEN iTHES Project and iTHEMS Program. We thank the JLQCD collaboration and CP-PACS collaboration for providing us their 2+1 flavor gauge configurations [45, 46]. The code for the eigenvectors of gauge covariant Laplacian was supplied by Colin Morningstar. We also thank for his kindness. All the numerical calculations are done on the Cray XC40 in Yukawa Institute for Theoretical Physics (YITP) in Kyoto University.

Appendix A: The maximum eigenvalue and the spatial distribution vs. the smearing level

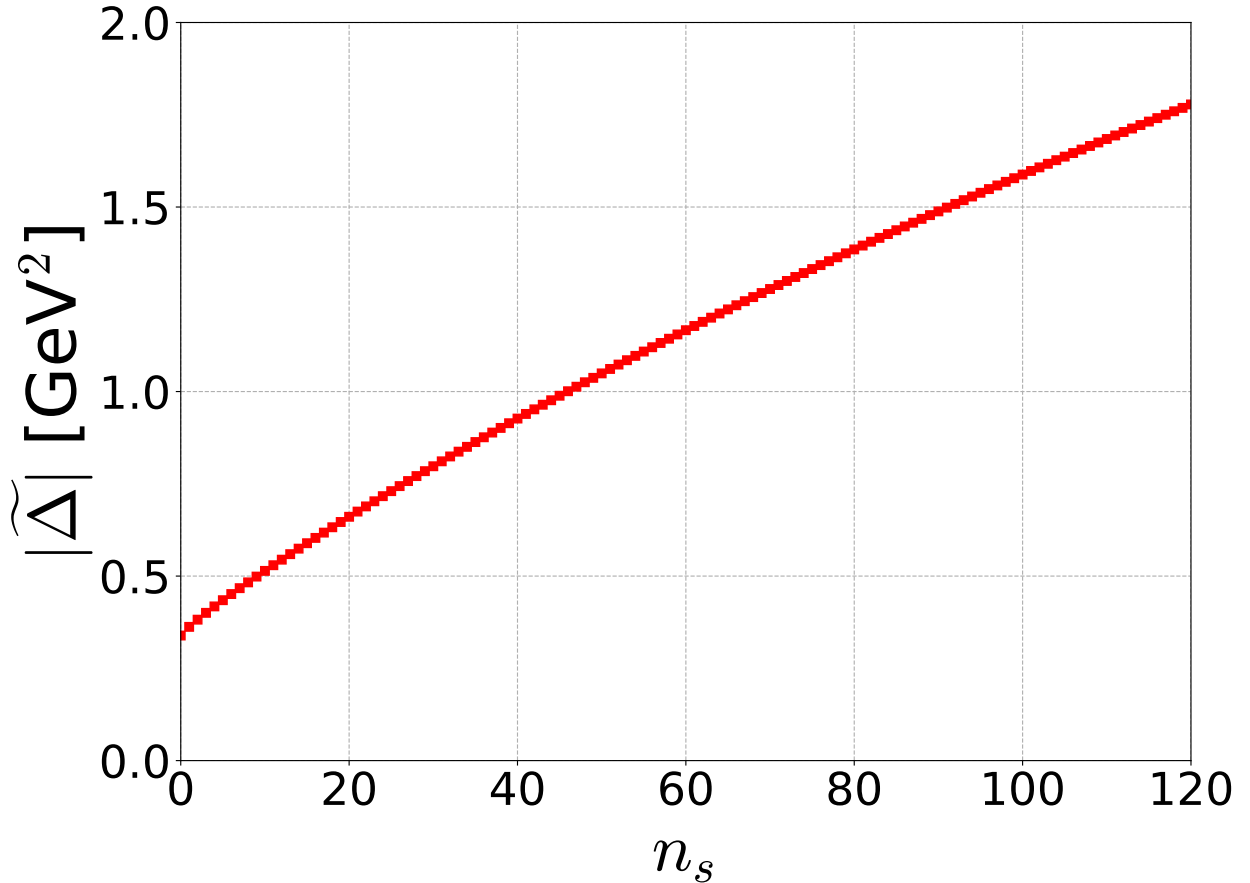


FIG. 7: The maximum eigenvalue of lattice covariant Laplacian $|\tilde{\Delta}|$ as a function of n_s .

Fig. 7 shows the maximum eigenvalue of the lattice covariant Laplacian in Eq. (23), $|\tilde{\Delta}|$

[GeV²], as a function of the smearing level n_s .

In Ref. [35], a measure of the spatial distribution for the LapH smearing is defined by

$$\Phi_{n_s}(\mathbf{r}) = \sum_{\mathbf{x}, t} \sqrt{\text{Tr} \{S_{n_s}(\mathbf{x}, \mathbf{x} + \mathbf{r}, t) S_{n_s}(\mathbf{x} + \mathbf{r}, \mathbf{x}, t)\}}, \quad (\text{A1})$$

which is gauge invariant and represents to what extent quark field is smeared. Fig. 8 gives this quantity for $n_s = 16, 32$, and 64. The figure tells us that the smeared quark is more localized as n_s increases.

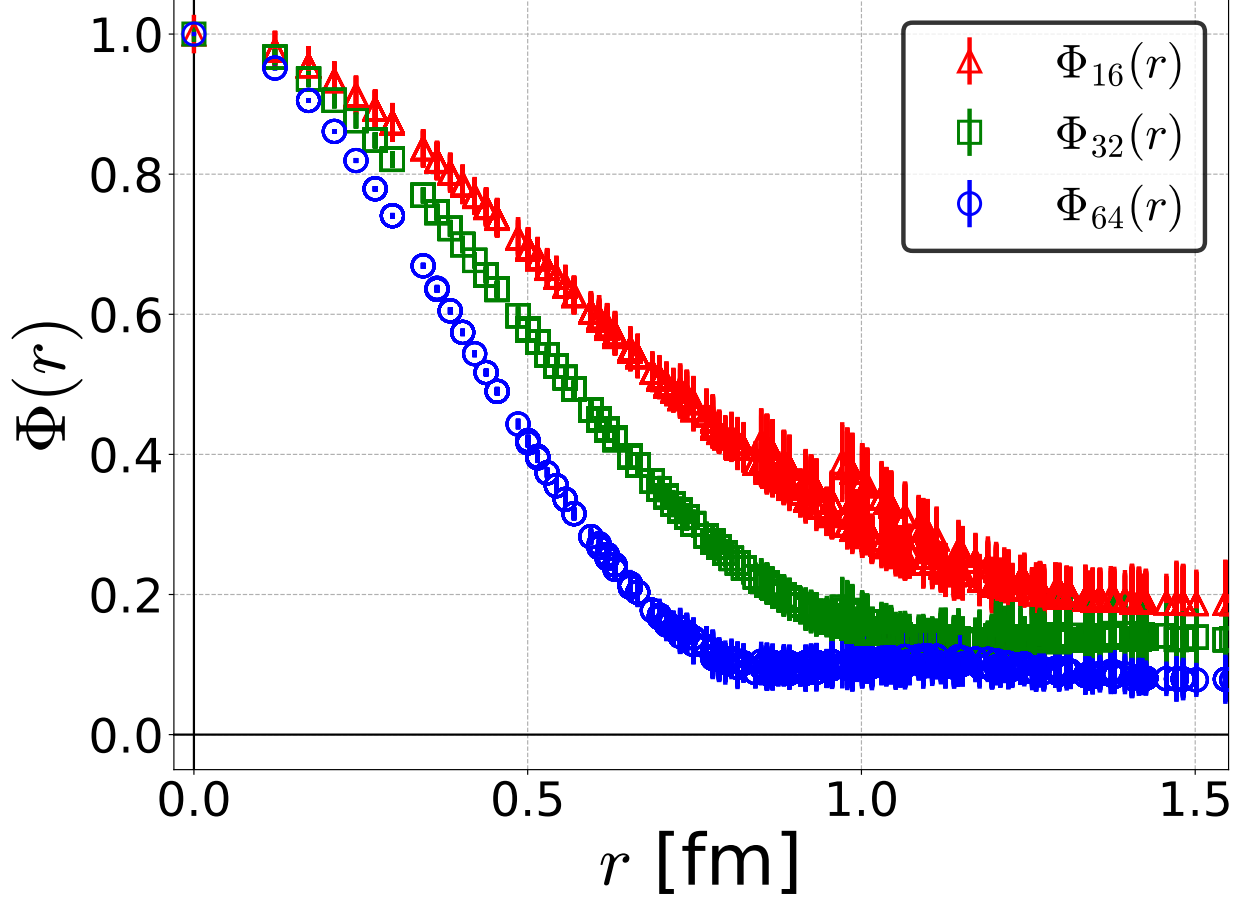


FIG. 8: A measure for the spatial distribution of LapH smearing operator.

Appendix B: Finite volume energies from the variational method

In the calculation of the finite volume energy, unwanted constant contribution from thermal quark loops to the 2-pion correlation function are removed as in Ref. [41],

$$\begin{aligned}\tilde{\mathcal{C}}_{n_a, n_b}^{4, \Lambda, \mu}(\mathbf{r}, t; |\mathbf{P}|, t_0) &= \mathcal{C}_{n_a, n_b}^{4, \Lambda, \mu}(\mathbf{r}, t; |\mathbf{P}|, t_0) \\ &\quad - \mathcal{C}_{n_a, n_b}^{4, \Lambda, \mu}(\mathbf{r}, t + \Delta t; |\mathbf{P}|, t_0),\end{aligned}\tag{B1}$$

where we set $\Delta t = 1$ in this paper.

In the variational method [13, 14], we consider the matrix

$$\begin{aligned}C(P, t, P', t_0) &= C(P, P_1; t_0)^{-\frac{1}{2}} \\ &\quad C(P_1, P_2; t)C(P_2, P'; t_0)^{-\frac{1}{2}},\end{aligned}\tag{B2}$$

where $C(P, P'; t)$ is given by the Fourier transformed 4-pt correlator

$$C(P, P'; t) = \sum_{\substack{t_1, t_2 \\ t=t_1-t_2}} \sum_{\substack{P \\ |P|:\text{fixed}}} \sum_{\mathbf{r}} e^{-i\mathbf{P}\cdot\mathbf{r}} \tilde{\mathcal{C}}_{n_a, n_b}^{4, A_1^+, 0}(\mathbf{r}, t_1; |\mathbf{P}'|, t_2).\tag{B3}$$

We denote $\lambda_n(t, t_0)$ as the eigenvalue of the matrix in Eq. (B2). The eigenenergy of the system E_n is extracted as

$$E_n = \lim_{t \rightarrow \infty} E_n(t), \quad E_n(t - t_0) \equiv -\frac{1}{t - t_0} \log \lambda_n(t, t_0),\tag{B4}$$

where we assume $E_0 \leq E_1 \leq E_2 \leq \dots$ and $E_n(t)$ is called the effective energy. In this study, we employ a 3×3 matrix from $P, P' = 0, 1, 2$ correlation functions with $n_a = n_b = 64$. Fig. 9 shows the effective energy $E_{0,1}(t - t_0)$ as a function of $t - t_0$.

Once E_n 's are obtained, phase shifts can be extracted by the Lüscher's finite volume method [1]. We calculate the momentum k^2 , which corresponds to the energy difference from the 2 pion mass, $k_n^2 = \frac{E_n^2}{4} - m_\pi^2$. As long as $l \geq 4$ partial waves are negligible, the Lüscher's formula for A_1^+ representation relates k_n^2 to the scattering phase shift as

$$k_n \cot \delta_0(k_n) = \frac{2\mathcal{Z}_{00}(1; q_n^2)}{\pi^{\frac{1}{2}} L},\tag{B5}$$

where L is the spatial lattice extension, q_n is the dimensionless momentum defined as $q_n \equiv k_n L / 2\pi$ and \mathcal{Z}_{00} is a generalized zeta function, $\mathcal{Z}_{00}(s, q^2) \equiv \frac{1}{\sqrt{4\pi}} \sum_{\mathbf{n} \in \mathbb{Z}^3} (\mathbf{n}^2 - q^2)^{-s}$.

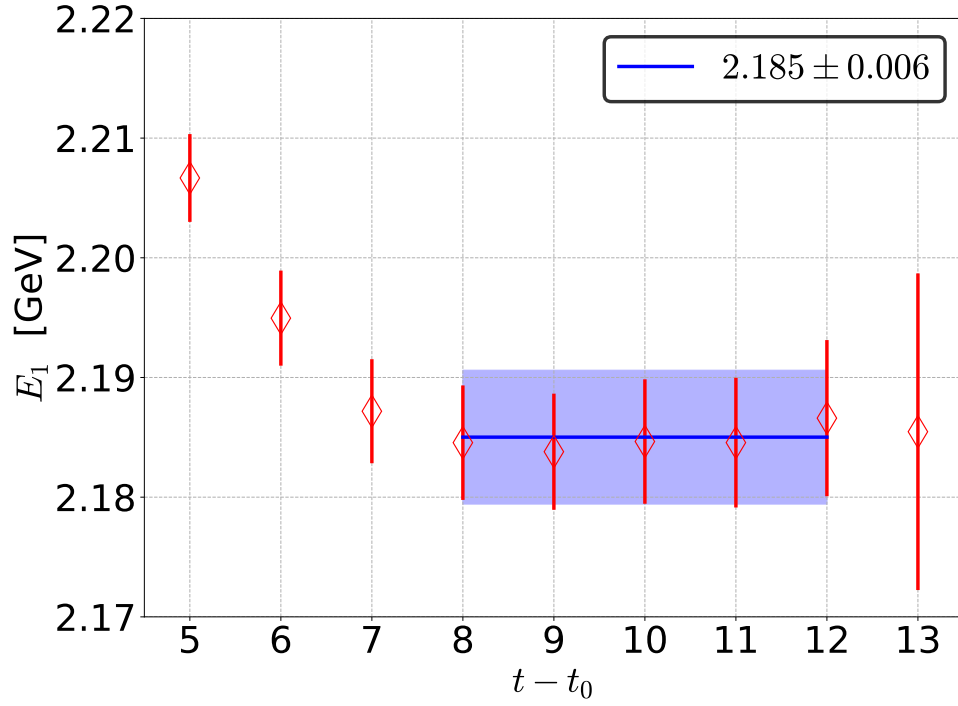
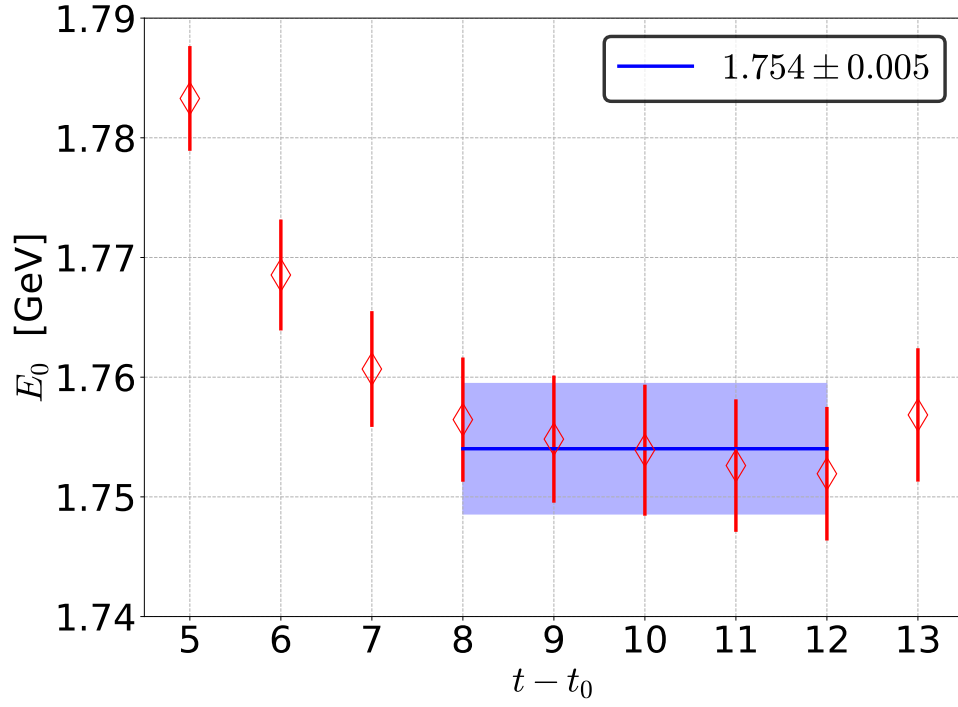


FIG. 9: The effective energy given by the variational method for $\tilde{\mathcal{C}}_{n_a, n_b}^{4, A_1^+, 1}(\mathbf{r}, t; |\mathbf{P}|, t_0)$. Upper and lower panel show the ground state energy and the first excited state energy, respectively. Blue solid lines with blue bands represent central values and errors from fits with data in these intervals.

Appendix C: Effective LO analysis in the smeared-sink scheme

As discussed in the main text (Sec. IV B), NLO correction is large in the smeared-sink scheme in particular at high energies, and the effective LO analysis is not sufficient. In this appendix, we nonetheless present the effective LO analysis in the smeared-sink scheme and demonstrate how the truncation error in the derivative expansion appears in the lattice QCD results.

1. Effective LO potentials

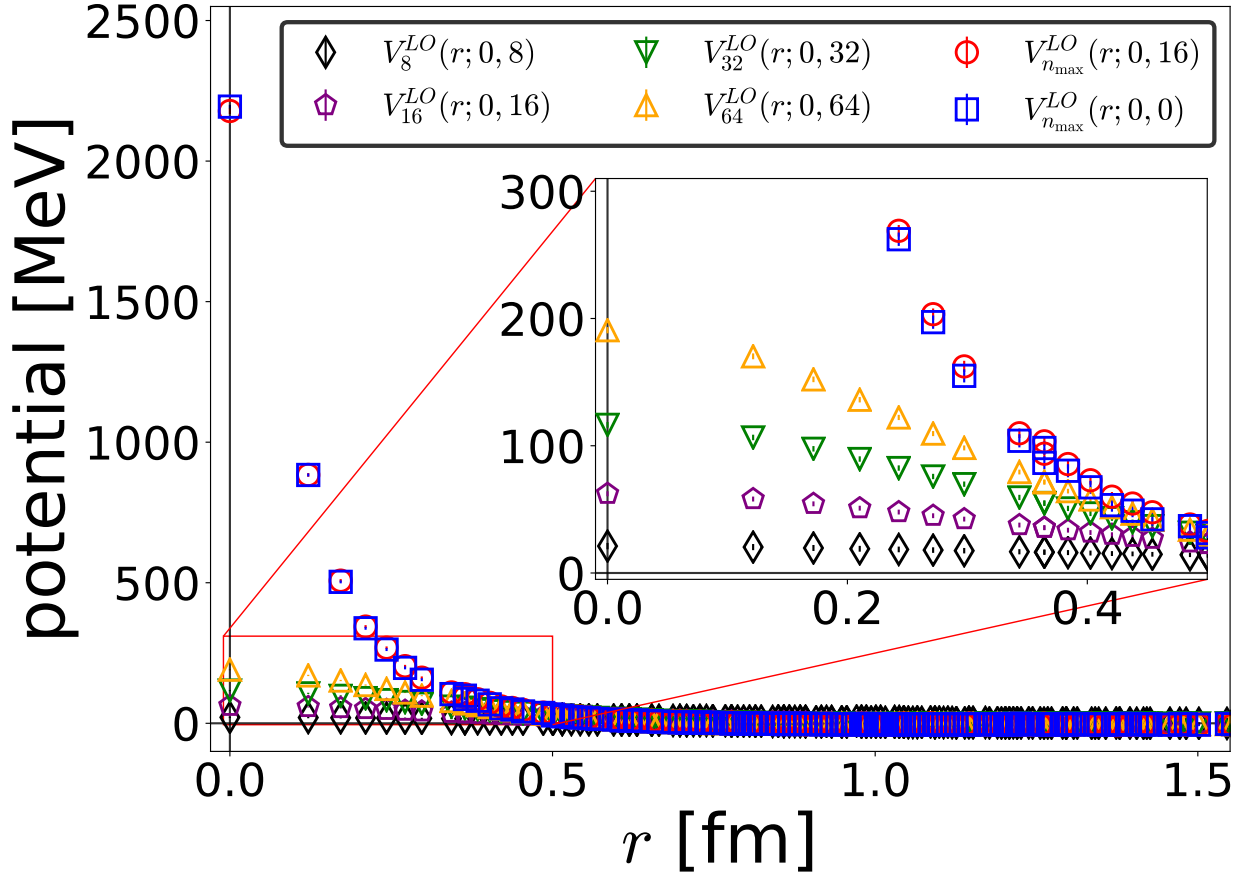


FIG. 10: The effective LO potential $V_{n_a}^{LO}(r; 0, n_b)$ for several combinations of (n_a, n_b) . Black diamonds, purple pentagons, green down triangles and orange up triangles correspond to $V_8^{LO}(r; 0, 8)$, $V_{16}^{LO}(r; 0, 16)$, $V_{32}^{LO}(r; 0, 32)$ and $V_{64}^{LO}(r; 0, 64)$, respectively, while red circles and blue squares give $V_{n_{max}}^{LO}(r; 0, 16)$ and $V_{n_{max}}^{LO}(r; 0, 0)$, respectively. The inset shows the comparison of the repulsion at short distance.

Fig. 10 shows the effective LO potential in the smeared-sink scheme $V_{n_a}^{\text{LO}}(r; 0, n_b)$ at $\mathbf{P} = [0, 0, 0]$, together with $V_{n_{\text{max}}}^{\text{LO}}(r; 0, n_b)$ for a comparison. As seen from the figure, effective LO potentials in the smeared-sink scheme have much reduced repulsive core than those in the point-sink scheme, while the long-distant part of the potential looks similar for all cases including the one in the point-sink scheme. We remind the readers that the potential is expected to be dependent on the scheme. In the inset of Fig. 10, a short distance part of potentials in the smeared-sink scheme is also shown. The magnitude of the potential at short distance increases monotonically as n_a increases (equivalently the size of the smearing range decreases as shown in Appendix. A).

2. Scattering phase shift

We study the S-wave $I = 2$ $\pi\pi$ scattering phase shifts $\delta_0(k)$ in the effective LO analysis. We extract the scattering phase shifts by solving the Schrödinger equation as described in Sec. II. We fit potentials in Fig. 10 with

$$V^{\text{LO}}(r) = A_1 e^{-\frac{r^2}{\sigma_1^2}} + A_2 e^{-\frac{r^2}{\sigma_2^2}} \quad (\text{C1})$$

for all r . Fig. 11 shows the phase shifts obtained from $V_{16}^{\text{LO}}(r; 0, 16)$ (purple), $V_{32}^{\text{LO}}(r; 0, 32)$ (green) and $V_{64}^{\text{LO}}(r; 0, 64)$ (orange), together with the benchmark result from $V_{n_{\text{max}}}^{\text{LO}}(r; 0, 16)$ (red), as a function of k^2 , where k is the magnitude of the scattering momentum.

Phase shifts in Fig. 11 show non-negligible dependence on the sink operator scheme. As the smearing level n_a increases, the phase shifts show more repulsive behavior and approach to the benchmark result in the point-sink scheme. The difference of the phase shifts between the smeared-sink scheme and the point-sink scheme is small at low energies but gradually become larger as k^2 increases. The discrepancy in phase shifts between the smeared sink and the point sink is originated from sizable NLO contributions in the smeared-sink scheme, which however decreases as n_a increases.

-
- [1] M. Lüscher, Nucl. Phys. B 354, 531 (1991).
 - [2] K. Rummukainen and S. Gottlieb, Nucl. Phys. B 450, (1995) 397-436.
 - [3] P. Guo, J. Dudek, R. Edwards and A. P. Szczepaniak, Phys. Rev. D 88, 014501 (2013).

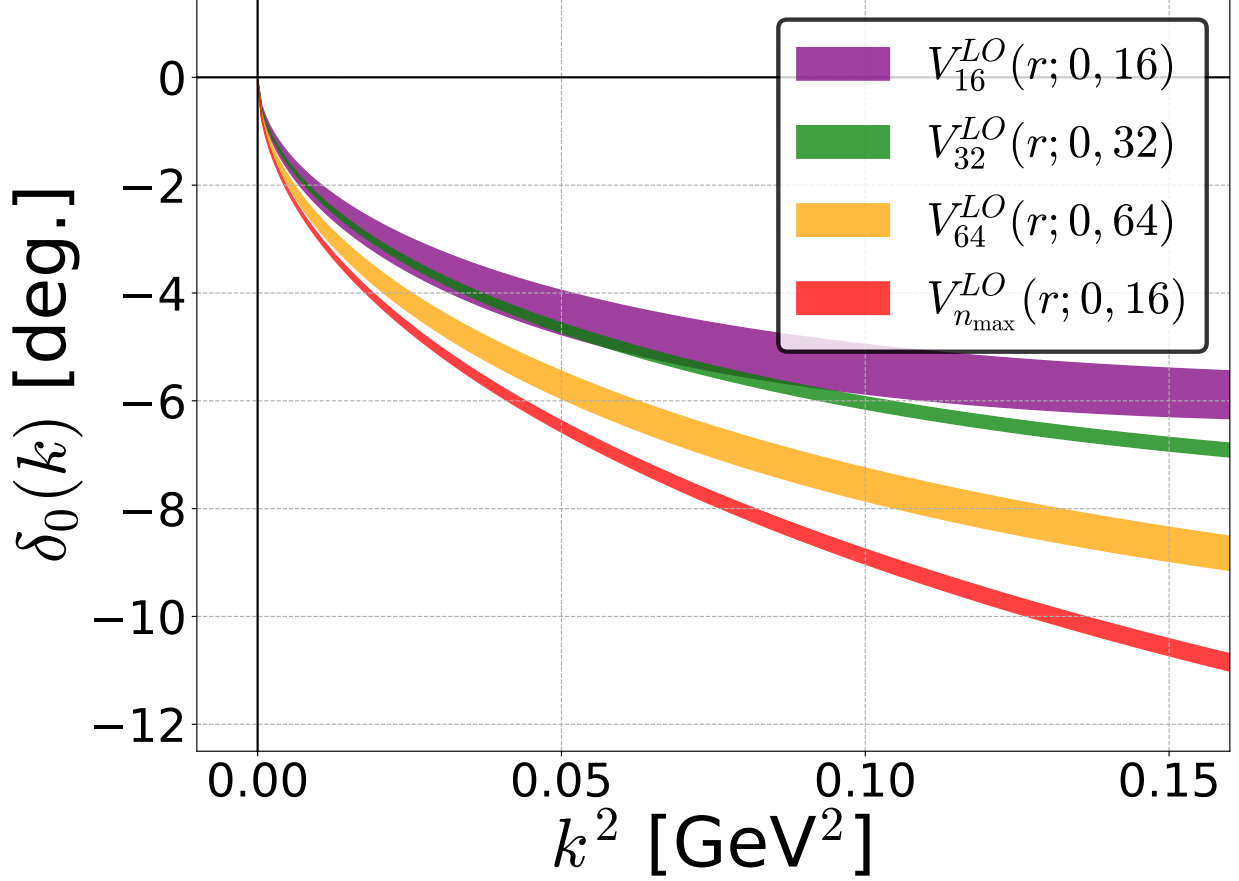


FIG. 11: The phase shifts of the S-wave $I = 2$ $\pi\pi$ scattering from the potential in the point-sink scheme (red) and the smeared-sink scheme with $n_a = n_b = 16$ (purple), 32 (green) and 64 (orange) as a function of k^2 .

- [4] S. He, X. Feng and C. Liu, JHEP 0507, (2005) 011.
- [5] R. A. Briceño and Z. Davoudi, Phys. Rev. D 88, 094507 (2013).
- [6] J. J. Dudek, R. G. Edwards, and C. E. Thomas (for the Hadron Spectrum Collaboration), Phys. Rev. D 87, 034505 (2013).
- [7] C. Helmes *et al.*, arXiv:1512.00282 [hep-lat].
- [8] R. A. Briceño, J. J. Dudek, R. G. Edwards and D. J. Wilson (for the Hadron Spectrum Collaboration), Phys. Rev. Lett. 118, 022002 (2017).
- [9] L. Liu *et al.* (ETM Collaboration), arXiv:1612.02061 [hep-lat].
- [10] R. A. Briceño, J. J. Dudek, R. G. Edwards and D. J. Wilson (for the Hadron Spectrum Collaboration), arXiv:1708.06667 [hep-lat].

- [11] R. A. Briceño *et al.* (for the Hadron Spectrum Collaboration), Phys. Rev. D 93, 094506 (2016).
- [12] Z.-H. Guo *et al.*, Phys. Rev. D 95, 054004 (2017).
- [13] C. Michael, Nucl. Phys. B 259, 58 (1985).
- [14] M. Lüscher and U. Wolff, Nucl. Phys. B 339, 222 (1990).
- [15] N. Ishii, S. Aoki and T. Hatsuda, Phys. Rev. Lett. 99, 022001 (2007).
- [16] S. Aoki, T. Hatsuda and N. Ishii, Prog. Theor. Phys. 123, 89 (2010).
- [17] N. Ishii *et al.* (HAL QCD Collaboration), Phys. Lett. B 712 (2012) 437.
- [18] S. Aoki, (for HAL QCD Collaboration), Prog. Part. Nucl. Phys. 66, 687 (2011).
- [19] S. Aoki *et al.* (HAL QCD Collaboration), Prog. Theor. Exp. Phys. 2012, 01A105 (2012).
- [20] T. Inoue *et al.* (HAL QCD Collaboration), Phys. Rev. Lett. 106, 162002 (2011).
- [21] T. Inoue *et al.* (HAL QCD Collaboration), Nucl. Phys. A 881, 28 (2012).
- [22] H. Nemura, N. Ishii, S. Aoki and T. Hatsuda, Phys. Lett. B 673, 136 (2009).
- [23] K. Murano, N. Ishii, S. Aoki and T. Hatsuda, Prog. Theor. Phys. 125, 1225 (2011).
- [24] K. Murano *et al.* (HAL QCD Collaboration), Phys. Lett. B 735, 19 (2014).
- [25] K. Sasaki *et al.* (HAL QCD Collaboration), Prog. Theor. Exp. Phys. 2015, 113B01 (2015).
- [26] Y. Ikeda *et al.*, Phys. Lett. B 729, 85 (2014).
- [27] F. Etminan *et al.* (HAL QCD Collaboration), Nucl. Phys. A 928, 89 (2014).
- [28] M. Yamada *et al.* (HAL QCD Collaboration), Prog. Theor. Exp. Phys. 2015, 071B01 (2015).
- [29] T. Doi *et al.* (for HAL QCD Collaboration), Prog. Theor. Phys. 127, 723 (2012).
- [30] T. Miyamoto *et al.* (HAL QCD Collaboration), arXiv:1710.05545 [hep-lat].
- [31] Y. Ikeda *et al.* (HAL QCD Collaboration), Phys. Rev. Lett. 117, 242001 (2016).
- [32] K. Nishijima, Phys. Rev. 111, 153 (1958).
- [33] W. Zimmermann, Nuovo Cimento 10, 597 (1958) and MPI-PAE/PTh-61/87 (1987) (unpublished).
- [34] R. Haag, Phys. Rev. 112, 669 (1958).
- [35] M. Peardon *et al.* (Hadron Spectrum Collaboration), Phys. Rev. D 80, 054506 (2009).
- [36] C. Morningstar *et al.*, Phys. Rev. D 83, 114505 (2011).
- [37] W. Hoogland *et al.*, Nucl. Phys. B 126, 109 (1977).
- [38] D. H. Cohen, T. Ferbel, P. Slattery, and B. Werner, Phys. Rev. D 7, 661 (1973).
- [39] N. Durusoy *et al.*, Phys. Lett. B 45, 517 (1973).
- [40] J. J. Dudek *et al.* (for the Hadron Spectrum Collaboration), Phys. Rev. D 83, 071504 (2011).

- [41] J. J. Dudek, R. G. Edwards, and C. E. Thomas (for the Hadron Spectrum Collaboration), Phys. Rev. D 86, 034031 (2012).
- [42] T. Kurth, N. Ishii, T. Doi, S. Aoki and T. Hatsuda, JHEP 12, (2013) 015.
- [43] T. Yamazaki and Y. Kuramashi, arXiv:1709.09779 [hep-lat].
- [44] C. Morningstar and M. J. Peardon, Phys. Rev. D 69, 054501 (2004).
- [45] S. Aoki *et al.* (JLQCD Collaboration), Phys. Rev. D 65, 094507 (2002).
- [46] T. Ishikawa *et al.* (CP-PACS, JLQCD Collaboration), Phys. Rev. D 73, 034501 (2006).